CrossMark

ORIGINAL PAPER

Theoretical insight into the interaction between SnX$_2$ (X=H, F, Cl, Br, I) and benzene

Piotr Matczak[1]

Abstract For a series of five model complexes composed of a singlet SnX$_2$ molecule (X=H, F, Cl, Br, I) and a benzene molecule, the first-principles calculations of their energetics and the analysis of their electron density topology have been performed. The CCSD(T)/CBS interaction energy between SnX$_2$ and C$_6$H$_6$ fall into the range between −10.0 and −11.2 kcal/mol, which indicates that the complexes are rather weakly bound. The relevant role of electrostatic and dispersion contributions to the interaction energy between SnX$_2$ and C$_6$H$_6$ is highlighted in the results obtained from the symmetry-adapted perturbation theory (SAPT). The electron density topological analysis has been carried out using the quantum theory of atoms in molecules (QTAIM) and the noncovalent interactions (NCI) visualization index. Both QTAIM and NCI prove the closed-shell, noncovalent and attractive character of the interaction. A very small charge transfer from C$_6$H$_6$ to SnX$_2$ has been detected. The formation of the five complexes is accompanied by the electron density deformations that are spatially restricted mostly to the region around the Sn atom and its adjacent C atom. The results presented in this work shed some light on the nature of the interactions associated with crystalline structural motifs involving low-valent tin complexed with neutral aryl rings.

✉ Piotr Matczak
  p.a.matczak@gmail.com

[1] Department of Theoretical and Structural Chemistry, Faculty of Chemistry, University of Łódź, Pomorska 163/165, 90-236 Lodz, Poland

Introduction

Interaction between metals and π-electron systems of neutral aryl rings is an interesting bonding motif for supramolecular self-assembly [1]. For instance, various transition metals interacting with benzene rings form both simple π-complexes in the gas phase [2–4] and larger supramolecular structures with this bonding motif [5–7]. However, the knowledge on the complexes of the heavier metals of groups 13–16 with neutral arenes is rather limited [8]. Tin is a good example in this context. The results of crystallographic studies [9] indicate that intermolecular Sn···π interactions often involve low-valent tin atoms, and therefore the complexation of stannylenes [10] by neutral aryl rings has attracted much interest in recent years [11–14].

  In this work, a series of five systems composed of a singlet tin(II) dihydride or dihalide SnX$_2$ (X=H, F, Cl, Br, I) molecule and a benzene molecule is considered. From a computational viewpoint, such systems may be regarded as model systems that approximate real systems in which the complexation of stannylenes by the π-electron cloud of neutral aryl rings occurs [9]. We focus mostly on the energetic and electron density topological description of the interaction between SnX$_2$ and C$_6$H$_6$ in the resulting complexes: SnH$_2$···C$_6$H$_6$ (**1**), SnF$_2$···C$_6$H$_6$ (**2**), SnCl$_2$···C$_6$H$_6$ (**3**), SnBr$_2$···C$_6$H$_6$ (**4**), and SnI$_2$··· C$_6$H$_6$ (**5**). Such quantum-chemical theories as the symmetry-adapted perturbation theory [15, 16] in both its traditional formulation (HF-SAPT) and its variant based on the density functional theory (DFT-SAPT), the quantum theory of atoms in molecules (QTAIM) [17], and the noncovalent interactions (NCI) visualization index

[18] are used to provide an in-depth insight into this inter-action. The present investigation is an extension of our previous work [19] in which only limited characteristics of **1–5** were obtained because some basic geometrical and energetic parameters were sufficient for our benchmark assessment of the accuracy of the Møller–Plesset second-order perturbation theory (MP2) and the density functional theory (DFT). There is also another theoretical study of the interaction of SnX_2 with C_6H_6 [20]. In that study, the properties of various SnX_2 molecules were characterized by conceptual DFT reactivity indices and the complexation of SnX_2 with a series of potential aromatic π-donors was examined. In particular, it was deduced from the results of natural bond orbital (NBO) calculations that the most important orbital interaction for this complexation was the overlap of the formally empty p-orbital on the Sn atom and the π-orbitals of the C_6H_6 molecule. Here, we employ not only a wide variety of first-principles methods for inspecting the energetics of the interaction between SnX_2 and C_6H_6 but additionally we explore the interaction in the complexes **1–5** from the perspective of their electron density topology.

Computational details

The geometries of **1–5** are taken from our previous study [19] in which they were optimized at the ωB97X/aug-cc-pVTZ(-PP) level of theory [21–24]. These geometries are character-ized by the absence of imaginary vibrational frequencies and they correspond to global minima on the potential energy surfaces of **1–5** (see also section S1 in Electronic Supplementary Material). Throughout this entire work, the aug-cc-pVTZ basis set [22] is ascribed to the atoms of H, C, F, Cl, and Br, whereas the aug-cc-pVTZ-PP basis set [23] is used for Sn and I. Their 28 core electrons are described by the corresponding energy-consistent Stuttgart/Cologne MDF pseudopotentials [24]. These pseudopotentials allow us to in-directly account for relativistic effects in Sn and I.

The formation of each complex is characterized by its com-plexation energy $E_{complex}$ that is defined as

$$E_{complex} = E_{def} + E_{int} + \Delta ZPVE \qquad (1)$$

where E_{def} is the so-called deformation energy needed to change the geometries of SnX_2 and C_6H_6 from those exhibited by isolated molecules to those observed in the complex, E_{int} is the interaction energy between SnX_2 and C_6H_6 in the complex and $\Delta ZPVE$ denotes the difference in the unscaled zero-point vibrational energies of the isolated SnX_2 and C_6H_6 molecules and the $SnX_2 \cdots C_6H_6$ complex. E_{int} can be computed using either supermolecular or perturbative approach. According to the former, subtracting the total energies of SnX_2 and C_6H_6 in

their geometries observed in the complex from the total energy of the $SnX_2 \cdots C_6H_6$ complex constitutes E_{int}. In this work, both DFT methods (such as SVWN [25, 26], BLYP [27, 28], B3LYP [28, 29], M06-2X [30] and ωB97X [21]), and wave function theory (WFT) methods (such as HF [31, 32], MP2 [33], SCS-MP2 [34], CCSD [35], and CCSD(T) [35]) are used to obtain E_{int} within the framework of the supermolecular approach. The E_{int} energies yielded by the HF and DFT methods are corrected for the basis set superposition error using the full counterpoise method of Boys and Bernardi [36]. The "half-half" counterpoise correction [37] is included in the E_{int} energies calculated using MP2, SCS-MP2, CCSD, and CCSD(T). The E_{int} energies at the CCSD(T) level of the-ory are additionally extrapolated to the complete basis set (CBS) limit via a composite scheme (for details, see section S2). The MP2, SCS-MP2, CCSD, and CCSD(T) methods make use of the frozen core approximation in the treatment of core electrons. All the calculations described in this paragraph have been done with Gaussian D.01 [38] and TURBOMOLE 6.6 [39] (for the DFT and WFT methods, respectively).

The SAPT method is used to determine the E_{int} energy between SnX_2 and C_6H_6 in a perturbative manner. Within the framework of this method, E_{int} is expressed as a sum of several energy terms that can be grouped into four principal components with clear physical meanings. The components covering exchange (E_{exch}), electrostatics (E_{elst}), induction (E_{ind}), and dispersion (E_{disp}) are assumed to include the fol-lowing energy terms occurring in the SAPT expansion of E_{int}:

$$E_{exch} = E_{exch}^{(1)} \qquad (2)$$

$$E_{elst} = E_{elst}^{(1)} \qquad (3)$$

$$E_{ind} = E_{ind}^{(2)} + E_{exch-ind}^{(2)} + \delta E_{HF} \qquad (4)$$

$$E_{disp} = E_{disp}^{(2)} + E_{exch-disp}^{(2)} \qquad (5)$$

The HF-SAPT [15, 16] and DFT-SAPT [40, 41] variants are employed. The gradient-regulated asymptotic correction of Grüning et al. [42] with the PBE0 functional [43] is intro-duced into the DFT-SAPT calculations of E_{int} in order to im-prove the asymptotic behavior of the DFT-SAPT variant. All the SAPT calculations have been performed using the MOLPRO 2012.1 program [44, 45].

The QTAIM analysis of the topology of the electron density in **1–5** and the calculations of QTAIM proper-ties have been done with the AIMAll 14.11.23 program [46]. The Multiwfn 3.3 program [47] has been used to perform the NCI analysis and to obtain a signature of electron pair distribution in terms of the electron local-ization function (ELF) [48]. The results are visualized using Jmol 14.2 [49], AIMStudio 14.11.23 [46], and VMD 1.9 [50].

Results and discussion

Structure and stability

Let us start by presenting the optimized geometries of **1**–**5**. All these complexes exhibit a marked structural similarity in which the SnX_2 molecule is arranged above the C_6H_6 ring (see Fig. 1a). The molecular plane of SnX_2 is approximately parallel to the plane of the C_6H_6 ring. All five complexes are of C_s symmetry. The Sn atom sits nearly on one of the C atoms, and the X atoms are directed outward the C_6H_6 ring. The distance between Sn and the C atom beneath ($d_{Sn\cdots C}$) falls in a narrow range between 2.919 and 3.076 Å (see Table S6 in Electronic Supplementary Material). This is much smaller than the sum of the Sn- and C-atom van der Waals radii (2.42 Å for Sn and 1.77 Å for C [51]). The values of the $a_{Sn\cdots C-H}$ angle do not differ significantly from 90°, and therefore, they indicate the η^1 type of complexation for **1**–**5**.

The aforementioned, almost parallel orientation of the SnX_2 and C_6H_6 molecular planes means that the formally empty p-orbital of the Sn atom is nearly perpendicular to the plane of the C_6H_6 ring. In such an orientation, the π-cloud overlaps the empty p-orbital effectively [20]. The lone electron pair of the Sn atom is positioned opposite the X atoms. Its localization is confirmed by the corresponding ELF isosurface depicted in Fig. 1b.

The comparison of the isolated SnX_2 and C_6H_6 molecules with the corresponding molecular fragments of **1**–**5** reveals that SnX_2 and C_6H_6 do not suffer any significant structural variations upon complexation (see Table S6). A minor effect of complexation on the geometries of SnF_2 and C_6H_6 molecular fragments constituting a 1:1 complex was confirmed experimentally, using matrix IR spectroscopy [52]. The vibrational frequencies measured for this complex were close to those of SnF_2 and benzene substrates, and on this basis, only a slight distortion of SnF_2 and C_6H_6 geometries was deduced. The complexation of Sn(II) by a six-membered aromatic ring

was also detected in several crystal structures [11–14]. The structures often revealed the η^6 type of Sn(II) complexation, with the distances between Sn(II) and the centroid of the interacting aromatic ring within the range from 3.2 to 4 Å [11, 12]. The lower end of this range is slightly larger than the $d_{Sn\cdots C}$ values found for **1**–**5**. Such a shortening of the distance between Sn(II) and the molecular plane of aromatic ring is a consequence of the η^1 type of complexation in **1**–**5**.

Energetic effects associated with the complexation of SnX_2 with C_6H_6 are summarized in Table 1. As evidenced by the values of $E_{complex}$, the formation of **1**–**5** from the isolated SnX_2 and C_6H_6 molecules is energetically favorable (that is, $E_{complex} < 0$), although the resulting stabilization of the complexes does not exceed several kcal/mol. The complexation of SnH_2 turns out to be slightly less energetically favorable than the complexation of tin(II) dihalides. The values of E_{def} are small, which is a consequence of the minor structural reorganization of SnX_2 and C_6H_6 upon complexation. For all five complexes, the interaction energy E_{int} contributes most to $E_{complex}$. The values of E_{int} fall in a narrow range between −9.1 and −9.7 kcal/mol, which obviously suggests that the interaction between SnX_2 and C_6H_6 in **1**–**5** is in fact quite similar. The difference in the energetics of the complexes becomes more significant with the $\Delta ZPVE$ component included.

The E_{int} values shown in Table 1 indicate that the interaction between SnX_2 and C_6H_6 can be classified into the category of weak intermolecular interactions. The interaction investigated here turns out to be much weaker than those involving benzene and alkali or alkaline-earth metal cations [53, 54] but stronger than the interactions in $SF_2\cdots C_6H_6$ [55] and $SeY_2\cdots C_6H_6$ (Y = H, F, Cl) [56].

The interaction energies of **1**–**5** have also been computed at various DFT and WFT levels, all using the geometries optimized by $\omega B97X/aug$-cc-pVTZ(-PP). The calculated values of E_{int} are reported in Table 2 (the E_{int} values that are uncorrected by the counterpoise method can be found in Table S7).

Fig. 1 Optimized geometry of **1** with two characteristic geometrical parameters marked (**a**) or ELF isosurfaces shown (**b**). These isosurfaces are plotted with a contour value of 0.85
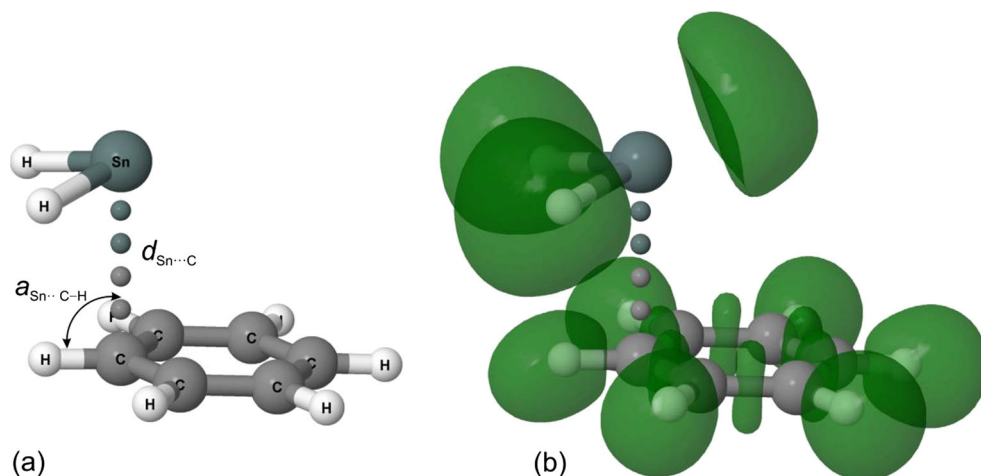
(a)   (b)

Table 1 Complexation energies and their components calculated using the ωB97X method

Energy	Complex				
	1	**2**	**3**	**4**	**5**
E_{def}	0.1	0.2	0.3	0.4	0.3
E_{int}	−9.3	−9.7	−9.7	−9.5	−9.1
$\Delta ZPVE$	1.6	0.7	0.6	0.6	0.6
$E_{complex}$	−7.6	−8.8	−8.8	−8.5	−8.2

All values in kcal/mol

We now test the reliability of the E_{int} energies obtained from less computationally expensive levels of theory against the CCSD(T)/CBS results.

The HF method predicts that the interaction between SnX_2 and C_6H_6 leads to the stabilization of **1–5** but the resulting E_{int} values are very small. Thus, the omission of electron correlation energy results in a major underestimation of the strength of the interaction between SnX_2 and C_6H_6.

The DFT methods present diverse performance, depending on the generation of a given DFT method. The SVWN functional leads to a typical overbinding [57]. In contrast to SVWN, the BLYP and B3LYP functionals predict that the complexes **1–5** are bound too weakly or even unbound (BLYP produces $E_{int} > 0$ for **5**). The E_{int} values obtained from B3LYP differ slightly from the corresponding B3LYP values reported in Ref. [20]. These differences originate from a greater number of core electrons described by the pseudopotential of Sn atom during the calculations carried out in Ref. [20]. A

Table 2 Interaction energies calculated using various methods

Method	Complex				
	1	**2**	**3**	**4**	**5**
HF	−2.1	−4.5	−2.9	−2.6	−2.1
SVWN	−14.5	−13.3	−13.1	−12.8	−12.2
BLYP	−3.3	−1.9	−0.9	−0.4	0.3
BLYP-D3(BJ)	−11.4	−10.8	−11.5	−11.6	−11.5
B3LYP	−4.6	−4.3	−3.2	−2.9	−2.2
B3LYP-D3(BJ)	−11.3	−11.7	−12.2	−12.2	−12.0
M06-2X	−10.4	−11.7	−11.1	−10.9	−10.8
ωB97X	−9.3	−9.7	−9.7	−9.5	−9.1
HF-SAPT	−11.6	−13.6	−13.7	−13.8	−13.6
DFT-SAPT	−8.8	−10.0	−10.4	−10.5	−10.3
MP2	−13.0	−13.1	−14.5	−14.6	−15.5
SCS-MP2	−10.5	−11.0	−11.9	−11.9	−12.5
CCSD	−9.2	−10.6	−10.4	−10.2	−10.7
CCSD(T)	−10.7	−11.6	−11.8	−11.7	−12.1
CCSD(T)/CBS	−10.0	−10.9	−11.2	−11.1	−11.1

All values in kcal/mol

common method that can improve the performance of BLYP and B3LYP in predicting the interaction energy of noncovalent complexes is to include an empirical dispersion correction. Here, Grimme's D3 term with Becke-Johnson damping (D3(BJ)) [58] is employed for BLYP and B3LYP. The application of the D3(BJ) term allows these two functionals to overcome the underestimation of E_{int} for **1–5**. However, both BLYP-D3(BJ) and B3LYP-D3(BJ) yield a minor overbinding in **1–5**, which suggests that the D3(BJ) term generally tends to overestimate slightly the role of long-range electron correlation in these complexes. This extends findings reported in a prior study [59]. It was shown therein that B3LYP combined with Grimme's dispersion correction yielded overbinding for hydrogen-bonded and ionic complexes. A slight overestimation of hydrogen-bond energy in DNA base pairs was also detected for the combination of BLYP with Grimme's dispersion correction [60, 61]. More recent DFT generations, represented in Table 2 by M06-2X and ωB97X, produce the E_{int} energies that mirror the CCSD(T)/CBS results fairly closely. It is known that the ωB97X functional has proved to be highly successful at providing accurate bond energies for compounds containing transition metals [62], as well as interaction energies for complexes of Sn(II) [19] and Sn(IV) [63, 64]. The good performance of M06-2X in predicting the E_{int} energies of **1–5** seems to confirm the important role of medium-range electron correlation for these complexes [30, 65].

As for the SAPT method, its HF-SAPT variant overestimates the strength of the interaction between SnX_2 and C_6H_6, while the DFT-SAPT variant demonstrates the opposite tendency. However, the former produces the E_{int} energies with worse accuracy relative to the CCSD(T)/CBS results than the latter does. It is so because the HF-SAPT variant applied here makes use of the simplest SAPT formulation, usually called HF-SAPT0 [66], that neglects the effects of intramonomer correlation. The intramonomer correlation effects are accounted for within the framework of the DFT-SAPT variant. It has been recently reported that DFT-SAPT generally underbinds H-bonded complexes [67] and it also proves to be the case with the interaction between SnX_2 and C_6H_6. The maximum DFT-SAPT underestimation of the strength of the interaction in **1–5** amounts to 1.2 kcal/mol — this is observed for **1**.

The performance of the advanced WFT methods also demonstrates some characteristic features. The MP2 method systematically overestimates the strength of the interaction between SnX_2 and C_6H_6 due to the omission of the repulsive intramolecular correlation correction within this method [68, 69]. The inclusion of Grimme's spin-component scaling (SCS) scheme [34] in the MP2 correlation energy reduces the overbinding of **1–5** but the E_{int} value of **5** is still overestimated by 1.4 kcal/mol. The overestimation occurring in SCS-MP2 results from the application of the "half-half"

correction of the basis-set superposition error. However, this correction leads to better agreement with the CCSD(T)/CBS interaction energies than the use of either uncorrected or full counterpoise-corrected values (see Table S8). Similarly to SCS-MP2, the CCSD(T) method also shows an overbinding tendency in E_{int}. Again, it is due to the application of the "half-half" correction. The E_{int} values yielded by CCSD are too small, which points at the importance of triple excitations in the correlation energy of **1**–**5**.

The CCSD(T)/CBS method, which is deemed to give the most accurate estimates of E_{int} in **1**–**5**, confirms that the interaction between SnX_2 and C_6H_6 should be classified as weak, with the E_{int} values between −10.0 and −11.2 kcal/mol. Comparing the CCSD(T)/CBS results with the ωB97X ones, we see that the former indicate a more diversified strength of the interaction in the investigated series of complexes. The $SnCl_2$ molecule is bound strongest to the C_6H_6 molecule, whereas the bonding of SnH_2 to C_6H_6 turns out to be particularly weak. For the complexes containing the tin(II) dihalides, no monotonous regularity in their CCSD(T)/CBS E_{int} values is found while X becomes heavier and heavier.

Interaction energy decomposition

The next step of this work is to characterize the physical nature of the interaction between SnX_2 and C_6H_6 using the SAPT method. We first focus on the DFT-SAPT interaction energy terms calculated for **1**–**5** and listed in Table 3. For all five complexes their electrostatic first-order term $E_{elst}^{(1)}$ is negative, which can be naively understood as a result of the attraction between the π-cloud and the positively-charged Sn atom (its QTAIM charge ranges from 0.86 to 1.49 au in **1**–**5**). The absolute values of $E_{elst}^{(1)}$ are always noticeably smaller than the corresponding values of the first-order exchange term $E_{exch}^{(1)}$. The magnitude of the second-order induction $E_{ind}^{(2)}$

$(SnX_2 \rightarrow C_6H_6)$ is several times larger than its $E_{ind}^{(2)}$ $(SnX_2 \leftarrow C_6H_6)$ analog. It means that the C_6H_6 molecule is easily polarized by the SnX_2 molecule, whereas the polarization in the opposite direction is significantly less pronounced. The $E_{ind}^{(2)}(SnX_2 \leftarrow C_6H_6)$ term of each complex is practically counterbalanced by the corresponding $E_{exch-ind}^{(2)}$ $(SnX_2 \leftarrow C_6H_6)$ term, while $E_{ind}^{(2)}(SnX_2 \rightarrow C_6H_6)$ is quenched up to ca. 66 % by its exchange counterpart. An even smaller percentage quenching of $E_{disp}^{(2)}$ is attributed to $E_{exch-disp}^{(2)}$. The δE_{HF} term destabilizes all five complexes. This term collectively gathers mostly third- and higher-order induction and exchange-induction contributions. The values of δE_{HF} decrease gradually in the sequence from **1** to **5**, that is, with growing $d_{Sn \cdots C}$ distance. This indicates that the higher-order effects become increasingly important at shorter distances. Even though the inclusion of δE_{HF} into the DFT-SAPT E_{int} values leads to the underestimation of the strength of the interaction in **1**–**5**, the presence of δE_{HF} is more beneficial for the accuracy of E_{int} than omitting this term. This is a well-documented feature of SAPT computations involving pseudopotentials [70].

Next, let us examine the relative importance of four principal components of E_{int} in order to establish the physical origin of the interaction between SnX_2 and C_6H_6. Table 4 summarizes the results of grouping either HF-SAPT or DFT-SAPT interaction energy terms into four principal components. We now take a closer look at the DFT-SAPT components but the findings we make using these components are also valid for the HF-SAPT components.

Table 3 SAPT interaction energy terms calculated using the DFT-SAPT variant

Energy term	Complex				
	1	**2**	**3**	**4**	**5**
$E_{exch}^{(1)}$	17.2	19.0	20.4	20.5	20.4
$E_{elst}^{(1)}$	−12.0	−14.0	−14.1	−14.0	−13.7
$E_{ind}^{(2)}(SnX_2 \rightarrow C_6H_6)$	−31.7	−28.1	−25.8	−24.6	−22.4
$E_{exch-ind}^{(2)}(SnX_2 \rightarrow C_6H_6)$	21.1	18.5	17.0	16.3	14.5
$E_{ind}^{(2)}(SnX_2 \leftarrow C_6H_6)$	−4.9	−6.0	−7.2	−7.8	−8.7
$E_{exch-ind}^{(2)}(SnX_2 \leftarrow C_6H_6)$	4.7	5.8	7.0	7.6	8.6
$E_{disp}^{(2)}$	−11.5	−11.6	−13.4	−13.9	−14.4
$E_{exch-disp}^{(2)}$	2.3	2.4	2.7	2.8	3.0
δE_{HF}	6.0	4.1	3.0	2.5	2.4

All values in kcal/mol

Table 4 Four principal components of SAPT interaction energies calculated using the HF-SAPT and DFT-SAPT variants

Principal component	Complex				
	1	**2**	**3**	**4**	**5**
$E_{exch}^{HF-SAPT}$	18.7	19.3	21.2	21.3	21.1
$E_{elst}^{HF-SAPT}$	−14.0 (46.2)	−16.1 (48.8)	−16.2 (46.4)	−16.0 (45.7)	−15.7 (45.1)
$E_{ind}^{HF-SAPT}$	−6.8 (22.6)	−7.7 (23.5)	−7.9 (22.6)	−7.9 (22.4)	−7.5 (21.6)
$E_{disp}^{HF-SAPT}$	−9.5 (31.2)	−9.1 (27.7)	−10.8 (31.0)	−11.2 (31.8)	−11.6 (33.3)
$E_{exch}^{DFT-SAPT}$	17.2	19.0	20.4	20.5	20.4
$E_{elst}^{DFT-SAPT}$	−12.0 (46.1)	−14.0 (48.4)	−14.1 (45.9)	−14.0 (45.1)	−13.7 (44.6)
$E_{ind}^{DFT-SAPT}$	−4.8 (18.3)	−5.7 (19.8)	−6.0 (19.4)	−6.0 (19.3)	−5.6 (18.3)
$E_{disp}^{DFT-SAPT}$	−9.3 (35.6)	−9.2 (31.8)	−10.7 (34.7)	−11.0 (35.6)	−11.4 (37.1)

The percentage share of individual attractive components in the total attraction between SnX_2 and C_6H_6 is given in parentheses

Energy components in kcal/mol

For all five complexes, the DFT-SAPT decomposition of their E_{int} energies yields three attractive components, namely $E_{elst}^{DFT-SAPT}$, $E_{ind}^{DFT-SAPT}$ and $E_{disp}^{DFT-SAPT}$. These three components provide sufficient stabilization to overcome the repulsive exchange component, and therefore, the resultant E_{int} values are negative (see Table 2). Among the attractive components, electrostatics represents the most energetically favorable contribution, followed by dispersion and then by induction. The $E_{elst}^{DFT-SAPT}$ component provides slightly less than half of the total attraction between SnX_2 and C_6H_6. However, this component does not surpass the $E_{exch}^{DFT-SAPT}$ one, and in consequence, the total contribution from the first-order DFT-SAPT energy terms remains repulsive. Therefore, the stability of 1–5 is due to the second- and higher-order DFT-SAPT energy terms, that are included in the $E_{ind}^{DFT-SAPT}$ and $E_{disp}^{DFT-SAPT}$ components. Of the two components, the latter plays the more important role. In relative terms, dispersion accounts for roughly one third of the total attraction between SnX_2 and C_6H_6. The relevant role of the dispersion energy often occurs for complexes containing large, diffuse electron clouds, such as the π-electron system of benzene in our case. The stabilization arising mainly from the combined effect of electrostatics and dispersion has recently been detected also for some other benzene complexes, e.g. with HCN [71].

The absolute values of $E_{ind}^{DFT-SAPT}$ essentially increase with the growing atomic number of the X atoms. However, there is a noticeable decrease of the magnitude of $E_{ind}^{DFT-SAPT}$ when one goes from 4 to 5. This results from the usage of a pseudopotential for the core electrons of the I atoms. For 2–5, the magnitude of $E_{disp}^{DFT-SAPT}$ and simultaneously the relative importance of this component increase while the halogen atoms get heavier. This is consistent with the growing polarizability of tin(II) dihalides [72]. In contrast to $E_{disp}^{DFT-SAPT}$, the other two attractive components of E_{int} show a diminishing relative importance while moving throughout the series from 2 to 5.

Topological analysis of electron density

Complementary information about the interaction between SnX_2 and C_6H_6 can be obtained from the QTAIM topological analysis of the electron density ρ in 1–5. The molecular graph determined for 1 is shown in Fig. 2. It is evident from the graph that there is a single bond path (BP) linking the Sn atom and the adjacent C atom of the C_6H_6 molecule. Such a feature of the topology of ρ is common to all five complexes 1–5. This suggests that the formation of a Sn$\cdots$C contact between the Sn atom and its nearest neighboring C atom of C_6H_6 is associated with the existence of a bonding interaction between these atoms [73]. The existence of the BP linking the Sn atom and its nearest neighboring C atom also indicates that, from the perspective of the QTAIM, the complexes 1–5 should be described as η^1 complexes.

The topological properties of ρ at the bond critical point (BCP) on the BP of the Sn$\cdots$C contact in 1–5 provide a more detailed QTAIM characteristics of the interaction between SnX_2 and C_6H_6. The values of several such properties are collected in Table 5. The values of ρ decrease with growing $d_{Sn\cdots C}$ distance. The relationship between ρ and $d_{Sn\cdots C}$ exhibits a good linear reverse correlation, with the respective coefficient of determination R^2 being equal to 0.96. It is due to the fact that the range of the $d_{Sn\cdots C}$ distances found for 1–5 is very narrow. For a broader range of distances a non-linear relationship should be rather expected, as it was demonstrated for other noncovalent interactions [74, 75]. The values of ρ at the BCP of the Sn$\cdots$C contact in 1–5 are much smaller than typical ρ values at the BCP of a covalent Sn-C bond (e.g. 0.099 and 0.106 au for the Sn-C bonds of $Sn(CH_3)_2$ and $Sn(CH_3)_4$, respectively). Furthermore, the ρ values in Table 5 are smaller than those found for Sn$\cdots$C contacts in the solid-state structure of dicationic tin-toluene complex $[Sn(C_7H_8)_3]^{2+}$ [13]. It is accompanied by an elongation of

Fig. 2 Molecular graph for 1. BCPs are denoted by small *red circles*, while the only ring critical point is marked by a small *yellow circle*. All atoms are colored the same as in Fig. 1
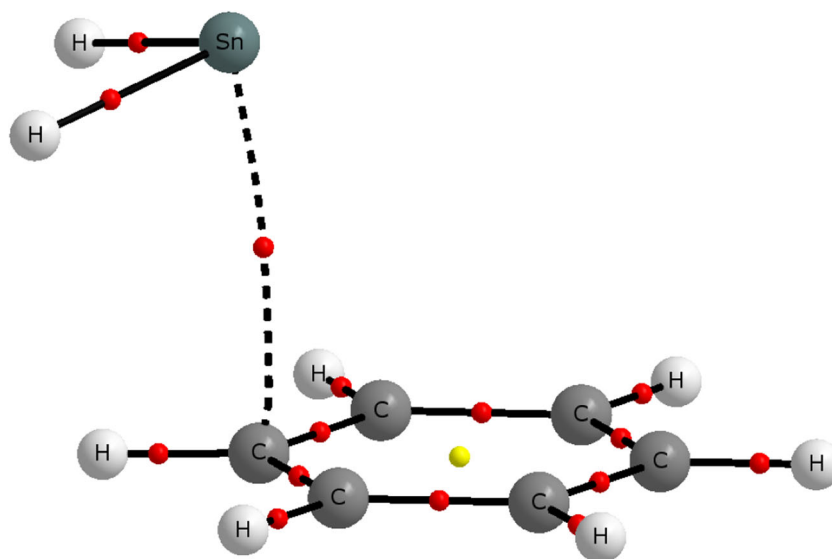
Table 5 QTAIM properties at the BCP on the BP linking the Sn atom and the adjacent C atom in each of the complexes **1**–**5**

Property	Complex				
	1	**2**	**3**	**4**	**5**
$\rho \cdot 10^2$	1.776	1.688	1.660	1.617	1.557
$\nabla^2\rho \cdot 10^2$	3.946	3.425	3.272	3.195	3.092
$G \cdot 10^3$	10.330	8.828	8.426	8.147	7.777
$V \cdot 10^3$	−10.795	−9.094	−8.674	−8.306	−7.825
$H \cdot 10^4$	−4.648	−2.661	−2.475	−1.587	−0.479
$-V/G$	1.045	1.030	1.029	1.019	1.006
$-\lambda_1/\lambda_3$	0.185	0.228	0.227	0.225	0.221

All values in au, except for the $-V/G$ and $-\lambda_1/\lambda_3$ ratios that are dimensionless

the $Sn \cdots C$ contact in **1**–**5** compared to the contacts of $[Sn(C_7H_8)_3]^{2+}$. The values of the Laplacian of the electron density $\nabla^2\rho$ in **1**–**5** are positive, which means that the charge density is locally depleted at the BCP relative to the neighboring points in space and, in consequence, it is locally concentrated in the basins of the Sn and C atoms of the contact. The total energy density H, which is the sum of the electron kinetic energy density G and the electron potential energy density V, adopts the negative sign but the values of H are very close to zero. This may suggest that there is only a minor covalent factor contributing to the nature of the interaction between SnX_2 and C_6H_6. Moreover, the low values of ρ and $\nabla^2\rho > 0$, together with $-V/G > 1$ and $-\lambda_1/\lambda_3 << 1$, provide evidence for the lack of any appreciable covalency [17, 74]. The aforementioned criteria indicate that this interaction should be classed as the closed-shell, noncovalent interaction [17, 74]. The $-\lambda_1/\lambda_3$ criterion of the nature of interaction is calculated using the lowest λ_1 and highest λ_3 eigenvalues of the Hessian matrix of ρ. The QTAIM characteristics of the $Sn \cdots C$ bonding interaction in **1**–**5** is essentially similar to that found previously for metal-ligand bonds in some complexes of Mn [76, 77] and Zn [78].

The standard QTAIM characterization presented above can be supplemented by the analysis of the NCI visualization index. The plots showing the NCI isosurfaces detected for **1**, **2**

and **5** are presented in Fig. 3. As can be seen in these plots, the interaction between SnX_2 and C_6H_6 in the complexes is characterized by a blue isosurface located between the Sn atom and its nearest neighboring C atom. The region delineated by this isosurface illustrates the occurrence of the attractive interaction between SnX_2 and C_6H_6. For the complexes containing the tin(II) dihalides, additional isosurfaces representing the interaction between SnX_2 and C_6H_6 appear. Such isosurfaces are located between the Sn atom and the more distant C atoms of C_6H_6. These isosurfaces are colored in green in Fig. 3 and they are associated with the occurrence of an extremely weak, repulsive interaction. Some other NCI isosurfaces denoting the existence of a secondary attractive interaction can in turn be found between the I atoms and their nearest neighboring H atoms in **5**. One may speculate that these isosurfaces can be ascribed to the occurrence of a very weak H-bonding, although no BP has been detected between the I and H atoms, and the distance of 3.651 Å between these atoms exceeds the sum of their van der Waals radii.

Electron density deformations and charge transfer

In the subsection presented above, the complexes have been examined mainly from the perspective of their ρ itself. Now, the comparison of this ρ with the electron densities of non-interacting SnX_2 and C_6H_6 fragments is made in order to determine how the electron density adjusts to the interaction between SnX_2 and C_6H_6. Such a comparison can conveniently be presented in the form of an electron density difference plot, as it is shown in Fig. 4 for **1**, **2** and **5**. For each of these complexes, its electron density difference has been computed as the difference between the ρ of the whole complex and the sum of the densities of individual SnX_2 and C_6H_6 fragments in their geometries taken from the complex. The regions delineated by blue isosurfaces in Fig. 4 illustrate an increase in ρ arising from the interaction, while the red regions determine where ρ is reduced. The most relevant changes in the ρ distribution are detected for the $Sn \cdots C$ contact and its spatially closest neighborhood. There is a region of ρ reduction immediately below the Sn atom of SnX_2, whereas an increase in ρ is observed above this atom. In other words, the ρ distribution
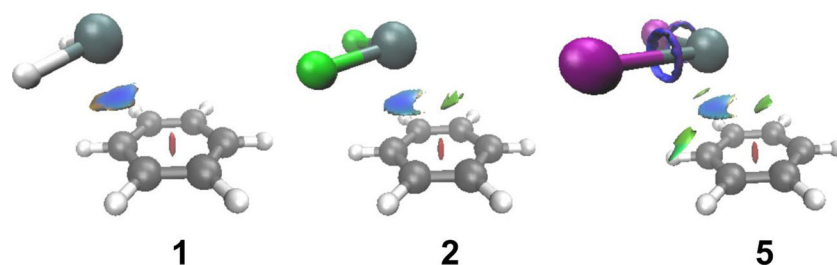

Fig. 3 NCI isosurfaces for **1**, **2** and **5**. The isosurfaces are plotted with a reduced density gradient value of 0.35 au and they are colored from blue to red according to sign(λ_2)ρ ranging from −0.02 to 0.02 au. The colors denoting the H, C and Sn atoms are the same as in Fig. 1. The atoms of F and I are drawn in green and violet, respectively

Fig. 4 Plots of the electron density difference calculated for **1**, **2** and **5**. The blue and red isosurfaces are plotted with contour values of 0.001 and −0.001 au, respectively. The colors coding individual elements are the same as in Fig. 3
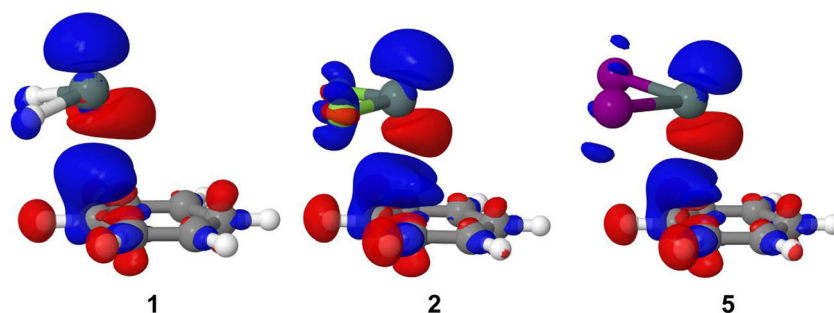
around the Sn atom becomes polarized toward the π-electron cloud of C_6H_6 upon complexation. The regions of growing ρ are found around the X atoms and the ρ deformation around these atoms is enhanced while moving from X = I to X = F, that is, with the increasing electronegativity of X. The distribution of ρ within the C_6H_6 molecule also undergoes some changes upon the complexation with SnX_2. The most prominent change can be perceived above the C atom involved in the contact with the Sn atom. The vast blue region of increased ρ spreads over the part of the adjacent C-H bond. This is accompanied by several regions of ρ loss around the H atoms on the periphery of C_6H_6.

An essential aspect of the interaction between SnX_2 and C_6H_6 is the magnitude of the charge transfer that possibly appears as a result of complexation. The charge transfer between SnX_2 and C_6H_6 is estimated here using the QTAIM atomic charges calculated for **1**–**5**. The QTAIM charges of atoms constituting the SnX_2 fragment of the complexes are summed up, yielding the overall magnitude of charge transferred between SnX_2 and C_6H_6. The magnitude of the charge transfer estimated in that manner adopts very small values, from 0.0388 au for **5** to 0.0578 au for **2**. The complexes containing the tin(II) dihalides show a gradual decrease in the magnitude of charge transfer while going throughout the series from **2** to **5**. For these complexes there is a strong linear association between the decreasing magnitude of charge transfer and the increasing value of $d_{Sn\cdots C}$ (the resulting inverse correlation between these two quantities is quantitatively characterized by $R^2 = 0.99$). The charge transfer in **1** is estimated to be 0.0415 au. The formation of all five complexes leads to a small flow of electron charge from the C_6H_6 molecule to the SnX_2 molecule. Thus, the SnX_2 fragment of **1**–**5** bears a slight negative charge, from −0.0388 to −0.0578 au. The detected very small charge transfer and its direction may point at the existence of a very weak donor-acceptor π → Sn contribution to the interaction in **1**–**5**. It would be in line with the results of a previous computational study based on the NBO approach [20]. In that study, an electron donation from the π-type NBO orbitals of C_6H_6 to the formally empty p-NBO orbital on the Sn atom of SnX_2 was indeed detected but the calculated charge transfers from C_6H_6 to SnX_2 were even smaller than those reported here.

Analysis of vibrational frequencies

The formation of **1**–**5** introduces some characteristic changes in the frequencies of vibrations occurring for the SnX_2 and C_6H_6 fragments of the complexes. Table 6 presents shifts in the frequencies of three vibrations upon complex formation. The three vibrations include asymmetrical and symmetrical stretching frequencies of Sn-X bonds ($\upsilon_{as,Sn\text{-}X}$ and $\upsilon_{s,Sn\text{-}X}$) and out-of-plane deformation vibrations of C-H bonds in the C_6H_6 ring ($\delta_{C\text{-}H}$). The frequencies of these vibrations have been computed within the quantum harmonic oscillator approximation at the ωB97X/aug-cc-pVTZ(-PP) level of theory. They have not been scaled.

The negative values of $\Delta\upsilon_{as,Sn\text{-}X}$ and $\Delta\upsilon_{s,Sn\text{-}X}$ shown in Table 6 indicate that small red shifts are observed for the frequencies of Sn-X stretching vibrations. The occurrence of these red shifts is associated with a minor elongation of Sn-X bonds upon complexation (see Table S6). The elongation of Sn-X bonds and the accompanying red shifts of Sn-X stretching frequencies can be roughly explained by the charge transfers between SnX_2 and C_6H_6. As it was discussed in the previous subsection, the SnX_2 fragment of the complexes bears a slight negative charge and the plots of the electron density difference show regions of electron accumulation around the Sn and X atoms upon complexation. Such a charge transfer contributes to the red shifts. The NBO results reported in Ref. [20] confirm the existence of the charge transfer from the π-type orbitals of C_6H_6 to the empty orbitals of SnX_2. Additionally, the charge transfer involving the π-type orbitals is reflected in the structural properties of the C_6H_6 ring. Our calculations reveal that the C-C bonds are elongated by ca. 0.002 Å upon the formation of $SnX_2 \cdots C_6H_6$. A region of growing ρ around the C atom adjacent to Sn has been clearly seen in Fig. 4. This implies that at the same time there is a reverse transfer toward C_6H_6, which also facilitates the red shifts. The NBO analysis has however established that the back-donation toward the π^*-orbitals of C_6H_6 is negligible in comparison to the transfer toward the orbitals of SnX_2 [20].

The calculated $\Delta\upsilon_{as,Sn\text{-}X}$, $\Delta\upsilon_{s,Sn\text{-}X}$ and $\Delta\delta_{C\text{-}H}$ of **2** can be compared with the corresponding experimental data taken from Ref. [52]. The calculated values demonstrate good agreement with the experimental data. The reliability of the

Table 6 Shifts in vibrational frequencies of **1**–**5** as the result of complex formation

Frequency shift	Complex				
	1	**2**	**3**	**4**	**5**
$\Delta\upsilon_{as,Sn-X}$	−41	−35 (−29)	−21	−15	−14
$\Delta\upsilon_{s,Sn-X}$	−38	−32 (−29)	−19	−12	−10
$\Delta\delta_{C-H}$	13	17 (19)	19	19	17

Available experimental results taken from Ref. [52] are given in parentheses

All values in cm^{-1}

presented computational predictions of shifts in vibrational frequencies can be further proven through the inclusion of additional complexes in this study. Two additional complexes composed of SnF_2 and chlorobenzene or toluene have been considered because their $\Delta\upsilon_{as,Sn-F}$, $\Delta\upsilon_{s,Sn-F}$ and $\Delta\delta_{C-H}$ shifts were previously determined experimentally [52]. The results obtained for these two additional complexes are presented in detail in section S3. Suffice it to say here that the calculated shifts in the Sn-F and C-H vibrational frequencies of **2** and two additional complexes are in good agreement with experiment. Moreover, the calculated shifts of $\upsilon_{as,Sn-F}$ and $\upsilon_{s,Sn-F}$ reproduce the experimentally established trend in the magnitude of these shifts [52].

Conclusions

In this work a variety of quantum-chemical methods have been used to provide an insight into the intermolecular interaction occurring in the complexes of SnX_2 with C_6H_6. By analyzing the results of energy and electron density topology calculations, we conclude with the following remarks.

1. The complexes are rather weakly bound and the E_{int} energy between SnX_2 and C_6H_6 turns out to be similar for all five complexes. A very small destabilizing effect associated with changes in the geometries of SnX_2 and C_6H_6 appears during the formation of each complex. This effect does not exceed 4 % of the absolute values of E_{int}.
2. The effects of electron correlation play a vital role in the proper description of the interaction in the five complexes. Among the DFT methods, those belonging to older DFT generations fail badly: both severe under- and overestimations of E_{int} are possible. The inclusion of the D3(BJ) correction improves their performance, but it tends to overestimate the role of long-range electron correlation. Newer density functionals without empirical dispersion

correction (M06-2X and ωB97X) acquit themselves reasonably well.
3. The SAPT analysis reveals that the electrostatics is the dominant attractive component of E_{int} for all five complexes. However, the E_{elst} component is compensated by the E_{exch} component, and therefore, the stabilization of the complexes is determined to a great extent by the second-order component that is accountable for dispersion.
4. Based on the QTAIM and NCI results, the interaction between SnX_2 and C_6H_6 can be classified as a closed-shell, noncovalent and attractive interaction. The formation of the complexes polarizes the electron density around the Sn atom toward the π-cloud of C_6H_6.
5. By integrating the electron density of the complexes over their QTAIM atomic basins, we have deduced a very small charge transfer from C_6H_6 to SnX_2 for all five complexes.
6. The calculated shifts in the frequencies of Sn-X and C-H vibrations agree well with the available experimental data. The relatively small shifts of these vibrational frequencies upon complexation confirm that the interaction between SnX_2 and C_6H_6 is rather weak and there is no appreciable change in the inner geometries of interacting SnX_2 and C_6H_6.

References

1. Haiduc I, Edelmann FT (1999) Supramolecular Organometallic Chemistry. Wiley-VCH, Weinheim
2. Meyer F, Khan FA, Armentrout PB (1995) Thermochemistry of transition metal benzene complexes: Binding energies of $M(C_6H_6)_x{}^+$ (x = 1,2) for M = Ti to Cu. J Am Chem Soc 117: 9740–9748
3. Kurikawa T, Takeda H, Hirano M, Judai K, Arita T, Nagao S, Nakajima A, Kaya K (1999) Electronic properties of organometallic metal-benzene complexes $[M_n(benzene)_m$ (M = Sc–Cu)]. Organometallics 18:1430–1438
4. Han S, Singh NJ, Kang TY, Choi K-W, Choi S, Baek SJ, Kim KS, Kim SK (2010) Aromatic π–π interaction mediated by a metal atom: Structure and ionization of the bis(η^6-benzene)chromium–benzene cluster. Phys Chem Chem Phys 12:7648–7653
5. Brunner H, Oescheya R, Nuber B (1996) Optically active transition metal complexes. Part 108. Synthesis, crystal structure and properties of a novel "quasi-meso" dinuclear η^6-benzene-ruthenium(II)

complex with chiral salicylaldiminato ligands. J Organomet Chem 518:47–53

6. Jiang J, Smith JR, Luo Y, Grennberg H, Ottosson H (2011) Multidecker bis(benzene)chromium: Opportunities for design of rigid and highly flexible molecular wires. J Phys Chem C 115:785–790

7. Haghiri A, Lerner H-W, Bats JW (2007) Tricarbonyl[η^6-1-methyl-4-(trimethylsilyl)benzene]chromium(0). Acta Cryst E 63:1133–1134

8. Schmidbaur H, Schier A (2008) π-Complexation of post-transition metals by neutral aromatic hydrocarbons: The road from observations in the 19th century to new aspects of supramolecular chemistry. Organometallics 27:2361–2395

9. Haiduc I, Tiekink ERT, Zukerman-Schpector J (2008) Intermolecular tin$\cdots\pi$-aryl interactions: Fact or artifact? A new bonding motif for supramolecular self-assembly in organotin compounds. In: Gielen M, Davies AG, Pannell KH, Tiekink ERT (eds) Tin Chemistry: Fundamentals, Frontiers, and Applications. John Wiley & Sons Ltd, Chichester, pp 392–412

10. Neumann WP (1991) Germylenes and stannylenes. Chem Rev 91:311–334

11. Zabula AV, Hahn FE (2008) Mono- and bidentate benzannulated N-heterocyclic germylenes, stannylenes and plumbylenes. Eur J Inorg Chem 2008:5165–5179

12. Mansell SM, Russell CA, Wass DF (2008) Synthesis and structural characterization of tin analogues of N-heterocyclic carbenes. Inorg Chem 47:11367–11375

13. Schäfer A, Winter F, Saak W, Haase D, Pöttgen R, Müller T (2011) Stannylium ions, a tin(II) arene complex, and a tin dication stabilized by weakly coordinating anions. Chem Eur J 17:10979–10984

14. Li J, Schenk C, Winter F, Scherer H, Trapp N, Higelin A, Keller S, Pöttgen R, Krossing I, Jones C (2012) Weak arene stabilization of bulky amido-germanium(II) and tin(II) monocations. Angew Chem Int Ed 51:9557–9561

15. Jeziorski B, Moszyński R, Szalewicz K (1994) Perturbation theory approach to intermolecular potential energy surfaces of van der Waals complexes. Chem Rev 94:1887–1930

16. Szalewicz K (2012) Symmetry-adapted perturbation theory of intermolecular forces. WIREs Comput Mol Sci 2:254–272

17. Bader RFW (1990) Atoms in Molecules: A Quantum Theory. Clarendon, Oxford, UK

18. Johnson ER, Keinan S, Mori-Sánchez P, Contreras-García J, Cohen AJ, Yang W (2010) Revealing noncovalent interactions. J Am Chem Soc 132:6498–6506

19. Matczak P, Wojtulewski S (2015) Performance of Møller-Plesset second-order perturbation theory and density functional theory in predicting the interaction between stannylenes and aromatic molecules. J Mol Model 21:41

20. Broeckaert L, Geerlings P, Růžička A, Willem R, De Proft F (2012) Can aromatic π-clouds complex divalent germanium and tin compounds? A DFT study. Organometallics 31:1605–1617

21. Chai J-D, Head-Gordon M (2008) Systematic optimization of long-range corrected hybrid density functionals. J Chem Phys 128:084106

22. Dunning TH Jr (1989) Gaussian basis sets for use in correlated molecular calculations. I. The atoms boron through neon and hydrogen. J Chem Phys 90:1007–1023

23. Peterson KA (2003) Systematically convergent basis sets with relativistic pseudopotentials. I. Correlation consistent basis sets for the post-d group 13–15 elements. J Chem Phys 119:11099–11112

24. Metz B, Stoll H, Dolg M (2000) Small-core multiconfiguration-Dirac–Hartree–Fock-adjusted pseudopotentials for post-d main group elements: Application to PbH and PbO. J Chem Phys 113:2563–2569

25. Slater JC (1974) The Self-Consistent Field for Molecular and Solids, Quantum Theory of Molecular and Solids, vol 4. McGraw-Hill, New York

26. Vosko SH, Wilk L, Nusair M (1980) Accurate spin-dependent electron liquid correlation energies for local spin density calculations: A critical analysis. Can J Phys 58:1200–1211

27. Becke AD (1988) Density-functional exchange-energy approximation with correct asymptotic behavior. Phys Rev A 38:3098–3100

28. Lee C, Yang W, Parr RG (1988) Development of the Colle–Salvetti correlation-energy formula into a functional of the electron density. Phys Rev B 37:785–789

29. Becke AD (1993) Density-functional thermochemistry. III. The role of exact exchange. J Chem Phys 98:5648–5642

30. Zhao Y, Truhlar DG (2008) The M06 suite of density functionals for main group thermochemistry, thermochemical kinetics, noncovalent interactions, excited states, and transition elements: Two new functionals and systematic testing of four M06-class functionals and 12 other functionals. Theor Chem Acc 120:215–241

31. Hartree DR (1928) The wave mechanics of an atom with a non-Coulomb central field. Part I: Theory and methods. Proc Cambridge Philos Soc 24:89–110

32. Fock V (1930) Näherungsmethode zur Lösung des quantenmechanischen Mehrkörperproblems. Z Phys 61:126–148

33. Møller C, Plesset MS (1934) Note on an approximation treatment for many-electron systems. Phys Rev 46:618–622

34. Grimme S (2003) Improved second-order Møller-Plesset perturbation theory by separate scaling of parallel- and antiparallel-spin pair correlation energies. J Chem Phys 118:9095–9102

35. Gauss J (1998) Coupled-cluster theory. In: Schleyer PR, Allinger NL, Clark T (eds) Encyclopedia of Computational Chemistry. John Wiley & Sons, Chichester, pp 615–636

36. Boys SF, Bernardi F (1970) The calculation of small molecular interactions by the differences of separate total energies. Some procedures with reduced errors. Mol Phys 19:553–566

37. Burns LA, Marshall MS, Sherrill CD (2014) Comparing counterpoise-corrected, uncorrected, and averaged binding energies for benchmarking noncovalent interactions. J Chem Theory Comput 10:49–57

38. Frisch MJ, Trucks GW, Schlegel HB, Scuseria GE, Robb MA, Cheeseman JR, Scalmani G, Barone V, Mennucci B, Petersson GA, Nakatsuji H, Caricato M, Li X, Hratchian HP, Izmaylov AF, Bloino J, Zheng G, Sonnenberg JL, Hada M, Ehara M, Toyota K, Fukuda R, Hasegawa J, Ishida M, Nakajima T, Honda Y, Kitao O, Nakai H, Vreven T, Montgomery JA Jr, Peralta JE, Ogliaro F, Bearpark M, Heyd JJ, Brothers E, Kudin KN, Staroverov VN, Keith T, Kobayashi R, Normand J, Raghavachari K, Rendell A, Burant JC, Iyengar SS, Tomasi J, Cossi M, Rega N, Millam JM, Klene M, Knox JE, Cross JB, Bakken V, Adamo C, Jaramillo J, Gomperts R, Stratmann RE, Yazyev O, Austin AJ, Cammi R, Pomelli C, Ochterski JW, Martin RL, Morokuma K, Zakrzewski VG, Voth GA, Salvador P, Dannenberg JJ, Dapprich S, Daniels AD, Farkas O, Foresman JB, Ortiz JV, Cioslowski J, Fox DJ (2013) Gaussian 09 D.01. Gaussian, Inc, Wallingford CT

39. Ahlrichs R, Armbruster MK, Bachorz RA, Bär M, Baron HP, Bauernschmitt R, Bischoff FA, Böcker S, Crawford N, Deglmann P, Della Sala F, Diedenhofen M, Ehrig M, Eichkorn K, Elliott S, Friese D, Furche F, Glöß A, Haase F, Häser M, Hättig C, Hellweg A, Höfener S, Horn H, Huber C, Huniar U, Kattannek M, Klopper W, Köhn A, Kölmel C, Kollwitz M, May K, Nava P, Ochsenfeld C, Öhm H, Pabst M, Patzelt H, Rappoport D, Rubner O, Schäfer A, Schneider U, Sierka M, Tew DP, Treutler O, Unterreiner B, von Arnim M, Weigend F, Weis P, Weiss H, Winter N (2014) TURBOMOLE 6.6. A development of University of Karlsruhe and Forschungszentrum Karlsruhe GmbH, 1989–2007, TURBOMOLE GmbH, since 2007, Karlsruhe, Germany, http://www.turbomole.com

40. Williams HL, Chabalowski CF (2001) Using Kohn–Sham orbitals in symmetry-adapted perturbation theory to investigate intermolecular interactions. J Phys Chem A 105:646–659

41. Jansen G, Hesselmann A (2001) Comment on "Using Kohn−Sham orbitals in symmetry-adapted perturbation theory to investigate intermolecular interactions". J Phys Chem A 105:11156–11157

42. Grüning M, Gritsenko OV, van Gisbergen SJA, Baerends EJ (2001) Shape corrections to exchange-correlation potentials by gradient-regulated seamless connection of model potentials for inner and outer region. J Chem Phys 114:652–660

43. Adamo C, Barone V (1999) Toward reliable density functional methods without adjustable parameters: The PBE0 model. J Chem Phys 110:6158–6170

44. Werner H-J, Knowles PJ, Knizia G, Manby FR, Schütz M, Celani P, Korona T, Lindh R, Mitrushenkov A, Rauhut G, Shamasundar KR, Adler TB, Amos RD, Bernhardsson A, Berning A, Cooper DL, Deegan MJO, Dobbyn AJ, Eckert F, Goll E, Hampel C, Hesselmann A, Hetzer G, Hrenar T, Jansen G, Köppl C, Liu Y, Lloyd AW, Mata RA, May AJ, McNicholas SJ, Meyer W, Mura ME, Nicklass A, O'Neill DP, Palmieri P, Peng D, Pflüger K, Pitzer R, Reiher M, Shiozaki T, Stoll H, Stone AJ, Tarroni R, Thorsteinsson T, Wang M (2012) MOLPRO 2012.1. University College Cardiff Consultants Limited, Cardiff, UK, http://www.molpro.net

45. Werner H-J, Knowles PJ, Knizia G, Manby FR, Schütz M (2012) MOLPRO: A general-purpose quantum chemistry program package. WIREs Comput Mol Sci 2:242–253

46. Keith TA (2014) AIMAll (Version 14.11.23). TK Gristmill Software, Overland Park KS, USA

47. Lu T, Chen F (2012) Multiwfn: A multifunctional wavefunction analyzer. J Comput Chem 33:580–592

48. Silvi B, Savin A (1994) Classification of chemical bonds based on topological analysis of electron localization functions. Nature 371:683–686

49. Jmol: An open-source Java viewer for chemical structures in 3D. http://www.jmol.org

50. Humphrey W, Dalke A, Schulten K (1996) VMD – Visual Molecular Dynamics. J Mol Graphics 14:33–38

51. Alvarez S (2013) A cartography of the van der Waals territories. Dalton Trans 42:8617–8636

52. Boganov SE, Egorov MP, Nefedov OM (1999) Study of complexation between difluorostannylene and aromatics by matrix IR spectroscopy. Russ Chem Bull 48:98–103

53. Soteras I, Orozco M, Luque FJ (2008) Induction effects in metal cation–benzene complexes. Phys Chem Chem Phys 10:2616–2624

54. Khanmohammadi A, Raissi H, Mollania F, Hokmabadi L (2014) Molecular structure and bonding character of mono and divalent metal cations (Li^+, Na^+, K^+, Be^{2+}, Mg^{2+}, and Ca^{2+}) with substituted benzene derivatives: AIM, NBO, and NMR analyses. Struct Chem 25:1327–1342

55. Nziko VPN, Scheiner S (2015) S···π Chalcogen bonds between SF_2 or SF_4 and C−C multiple bonds. J Phys Chem A 119:5889–5897

56. Saberinasab M, Salehzadeh S, Maghsoud Y, Bayat M (2016) The significant effect of electron donating and electron withdrawing substituents on nature and strength of an intermolecular Se···π interaction. A theoretical study. Comput Theoret Chem 1078:9–15

57. Kurth S, Perdew JP, Blaha P (1999) Molecular and solid-state tests of density functional approximations: LSD, GGAs, and meta-GGAs. Int J Quantum Chem 75:889–909

58. Grimme S, Ehrlich S, Goerigk L (2011) Effect of the damping function in dispersion corrected density functional theory. J Comput Chem 32:1456–1465

59. Schneebeli ST, Bochevarov AD, Friesner RA (2011) Parameterization of a B3LYP specific correction for noncovalent interactions and basis set superposition error on a gigantic data set of CCSD(T) quality noncovalent interaction energies. J Chem Theory Comput 7:658–668

60. van der Wijst T, Fonseca Guerra C, Swart M, Bickelhaupt FM, Lippert B (2009) A ditopic ion-pair receptor based on stacked nucleobase quartets. Angew Chem Int Ed 48:3285–3287

61. Fonseca Guerra C, van der Wijst T, Poater J, Swart M, Bickelhaupt FM (2010) Adenine versus guanine quartets in aqueous solution: Dispersion-corrected DFT study on the differences in π-stacking and hydrogen-bonding behavior. Theor Chem Acc 125:245–252

62. Zhang W, Truhlar DG, Tang M (2013) Tests of exchange-correlation functional approximations against reliable experimental data for average bond energies of 3d transition metal compounds. J Chem Theory Comput 9:3965–3977

63. Matczak P, Łukomska M (2014) Assessment of various density functionals for intermolecular N → Sn interactions: The test case of trimethyltin cyanide dimer. Comput Theoret Chem 1036:31–43

64. Matczak P (2015) Assessment of various density functionals for intermolecular N → Sn interactions: The test case of poly(trimethyltin cyanide). Comput Theoret Chem 1051:110–122

65. Zhao Y, Truhlar DG (2007) Density functionals for noncovalent interaction energies of biological importance. J Chem Theory Comput 3:289–300

66. Hohenstein EG, Sherrill CD (2012) Wavefunction methods for noncovalent interactions. WIREs Comput Mol Sci 2:304–326

67. Parker TM, Burns LA, Parrish RM, Ryno AG, Sherrill CD (2014) Levels of symmetry adapted perturbation theory (SAPT). I. Efficiency and performance for interaction energies. J Chem Phys 140, 094106

68. Cybulski SM, Chałasiński G, Moszyński R (1990) On decomposition of second-order Møller-Plesset supermolecular interaction energy and basis set effects. J Chem Phys 92:4357–4363

69. Cybulski SM, Lytle ML (2007) The origin of deficiency of the supermolecule second-order Møller-Plesset approach for evaluating interaction energies. J Chem Phys 127:141102

70. Patkowski K, Szalewicz K (2007) Frozen core and effective core potentials in symmetry-adapted perturbation theory. J Chem Phys 127:164103

71. Riley KE, Ford CL Jr, Demouchet K (2015) Comparison of hydrogen bonds, halogen bonds, C-H···π interactions, and C-X···π interactions using high-level ab initio methods. Chem Phys Lett 621:165–170

72. Kalugina YN, Thakkar AJ (2015) Electric properties of stannous and stannic halides: How good are the experimental values? Chem Phys Lett 626:69–72

73. Bader RFW (1998) A bond path: A universal indicator of bonded interactions. J Phys Chem A 102:7314–7323

74. Espinosa E, Alkorta I, Elguero J, Molins E (2002) From weak to strong interactions: A comprehensive analysis of the topological and energetic properties of the electron density distribution involving X–H···F–Y systems. J Chem Phys 117:5529–5542

75. Grabowski SJ, Leszczynski J (2009) The enhancement of X–H···π hydrogen bond by cooperativity effects — Ab initio and QTAIM calculations. Chem Phys 355:169–176

76. Bianchi R, Gervasio G, Marabello D (2000) Experimental electron density analysis of $Mn_2(CO)_{10}$: Metal-metal and metal-ligand bond characterization. Inorg Chem 39:2360–2366

77. Van der Maelen JF, Cabeza JA (2012) QTAIM analysis of the bonding in Mo−Mo bonded dimolybdenum complexes. Inorg Chem 51:7384–7391

78. Cukrowski I, de Lange JH, Mitoraj M (2014) Physical nature of interactions in Zn^{II} complexes with 2,2′-bipyridyl: Quantum theory of atoms in molecules (QTAIM), interacting quantum atoms (IQA), noncovalent interactions (NCI), and extended transition state coupled with natural orbitals for chemical valence (ETS-NOCV) comparative studies. J Phys Chem A 118:623–637